



Study of radiation build-up and spectral evolution in the Israeli electrostatic accelerator free-electron laser oscillator

A. Abramovich^{a,*}, Y. Pinhasi^b, Y. Yakover^a, A. Gover^a, J.S. Sokolowski^a,
M. Canter^a

^a*Faculty of Engineering, Tel-Aviv University, Physical Electronics, 69978 Ramat-Aviv, Israel*

^b*Faculty of Engineering, Department of Electrical and Electronic Engineering, The College of Judea and Samaria, Ariel, Israel*

Abstract

Time–frequency study of oscillation build-up in an electrostatic accelerator free-electron laser (EA-FEL) oscillator is presented. The unique features of EA-FEL and its capacity to operate in a long pulse mode, enable observation and study of linear and non-linear processes taking place in the evolution of radiation in the EA-FEL oscillator. The experimental data recorded with the aid of a digital 4 GS/s fast sampling oscilloscope, was analyzed using various signal processing techniques to obtain time–frequency phase space presentation of the power spectral density evolution. This presentation make it possible to follow the radiation field coherence evolution from noise to saturation including intermediate stages of mode build-up from noise and competition between longitudinal modes until single-mode steady-state operation is established. The experimental results were also compared with the results of a FEL oscillator simulation code. The code predicts well the behavior of the oscillator in its various regimes of operation. © 1999 Elsevier Science B.V. All rights reserved.

Keywords: Electrostatic accelerator-free electron laser; RF detector

1. Introduction

We report single mode and multimode operation of an electrostatic accelerator free electron laser (EA-FEL) oscillator using an internal cavity.

The FEL is based on the 6 MeV Tandem Van de Graaff accelerator of the Weizman Institute. It was

converted into a high-current electron beam accelerator, and was modified so as to enable the insertion of a magnetostatic wiggler containing a mm-wave resonator and electron-optical focusing elements in the positively charged HV terminal (see Fig. 1) [1,2]. The FEL is presently operating in a pulsed mode at 100 GHz. Table 1 summarizes the parameters of the EA-FEL.

Since the first lasing of the EA-FEL [3], we significantly improved the current control of the e-beam and the experimental instrumentation. These improvements enable us to increase the e-beam current through the wiggler to 1 A and to analyze the spectral components of the FEL radiation as function of time.

*Corresponding author. Tel.: + 972-3-640-8271; fax: + 972-3-642-3508.

E-mail address: amir007@eng.tau.ac.il (A. Abramovich)

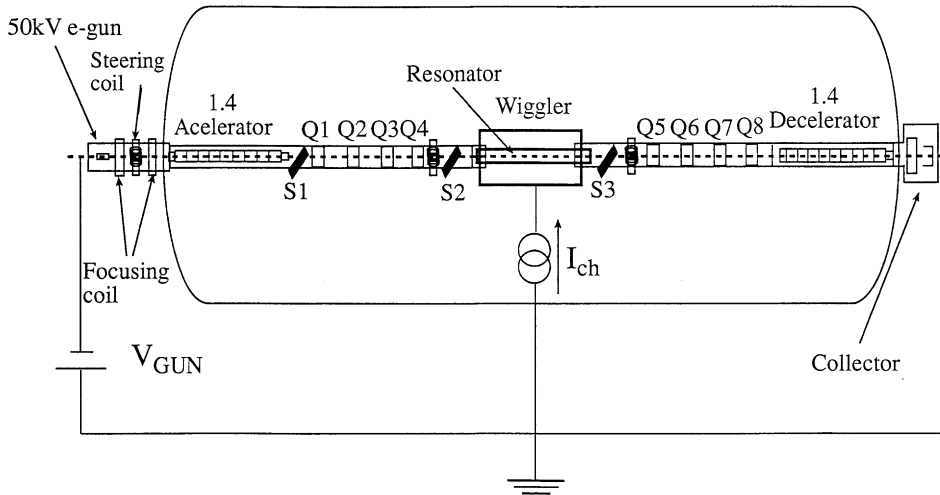


Fig. 1. Electron beam line of the Israeli EA-FEL.

Table 1
Parameters of the tandem FEL

<i>Accelerator:</i>	
Electron beam energy	$E_k = 1.4 \text{ MeV}$
Beam current	$I_0 = 1.5 \text{ A}$
<i>Wiggler:</i>	
Magnetic induction	$B = 2000 \text{ G}$
Period length	$\lambda_w = 4.4 \text{ cm}$
Number of periods	$N_w = 20$
<i>Waveguide resonator:</i>	
Curved parallel plate resonator	
Mode	TE_{01}
Total reflectivity	$R = 91\%$
Resonator length	$L_c = 130.8 \text{ cm}$
Quality factor	$A = 30,000$

2. Experimental setup

Fig. 1 shows the layout of the electron beam line along the FEL. The electron optics of this FEL is based on a straight line geometry and a positive HV terminal. The electron injection system is based on a 43 kV Pierce-type e-gun and employs focusing and steering coils after the cathode. The parallel-flow electron gun produces a high-quality electron beam (with emittance of $\epsilon_n = 10\pi \text{ mm mrad}$ [2]), which is injected to the acceleration section. The

following four quadrupole lenses (Q1–Q4) are used to control the e-beam and determine optimal entrance conditions to the wiggler [4]. The wiggler and the mm-wave resonator, forming the FEL interaction region, are installed inside the positively charged high voltage terminal, located at the center of the tank along the symmetry axis. The quadrupoles Q5, Q6, Q7 and Q8 collimate the e-beam into the deceleration section prior to collection by a depressed collector, which provides e-beam energy recuperation. Three diagnostic screens S1, S2 and S3 were used for monitoring of the e-beam transport.

A permanent magnet wiggler, arranged in a Halbach planar configuration [5] is employed. Two long magnets were used, one on each side of the wiggler, to focus the e-beam in the lateral (wiggling) plane by means of a lateral magnetic gradient which they produce on that axis [6]. The RF resonator utilizes curved parallel plates as a waveguide structure and has two quasioptical Talbot effect reflectors (wave splitters) one at each resonator end, which enable e-beam passage into and out of the resonator [7,8]. This type of resonator is characterized by very small ohmic and total radiation losses of about 9%, as was determined in Ref. [8] by loss measurements prior to the installation of the resonator in the HV terminal.

3. Experimental results

The EA-FEL was operated in a pulsed mode, using the current control electrode of the e-gun, to produce 20 μs duration e-beam pulses. The power and spectral evolution of the radiation build-up process were measured with the aid of the diagnostic setup shown in Fig. 2. Power measurements were made using the RF detector. Simultaneously, measurements of the IF signal were made, using a mixer and a local oscillator. Oscilloscope traces of the e-beam currents, RF power, and high voltage droop are shown in Fig. 3. Trace 1 is the voltage droop at the terminal during the e-beam pulse, trace 2 is the cathode current pulse, trace 3 is the power measured by the RF detector, and trace 4 is the e-beam current measured at the wiggler exit. The measurements show that the high voltage droop during an e-beam 20 μs pulse is about 22 kV. The e-beam current transiting the wiggler is about 1 A, and the RF output power is about 8 kW. The IF signal was recorded by a 4 Gsample/s digital oscilloscope and stored and processed in a PC computer.

4. Analysis and simulation

The time–frequency diagram shown in Fig. 4 includes frequencies obtained by mixing the local oscillator with the exited radiation of the longitudinal modes. Therefore, the intermediate frequency (IF) signal consists of down converted

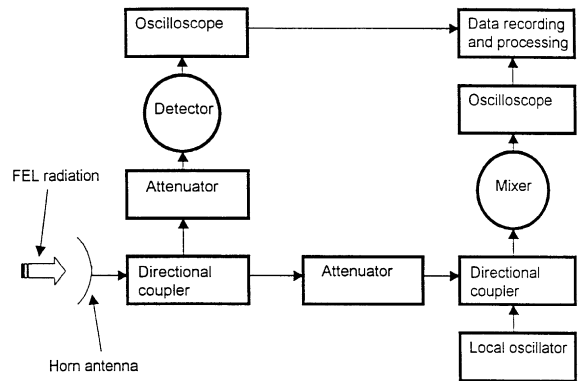


Fig. 2. Experimental setup for measuring the FEL RF power and spectral components of the radiation.

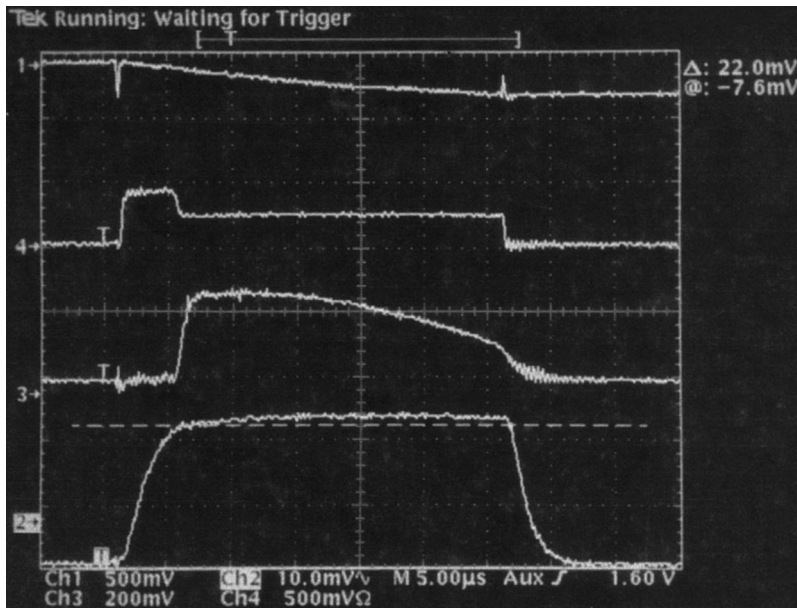


Fig. 3. Experimental measurements of high voltage droop (trace 1), E-beam current at the cathode (trace 2), output radiation power of the EA-FEL (trace 3) and e-beam current after interaction region (trace 4).

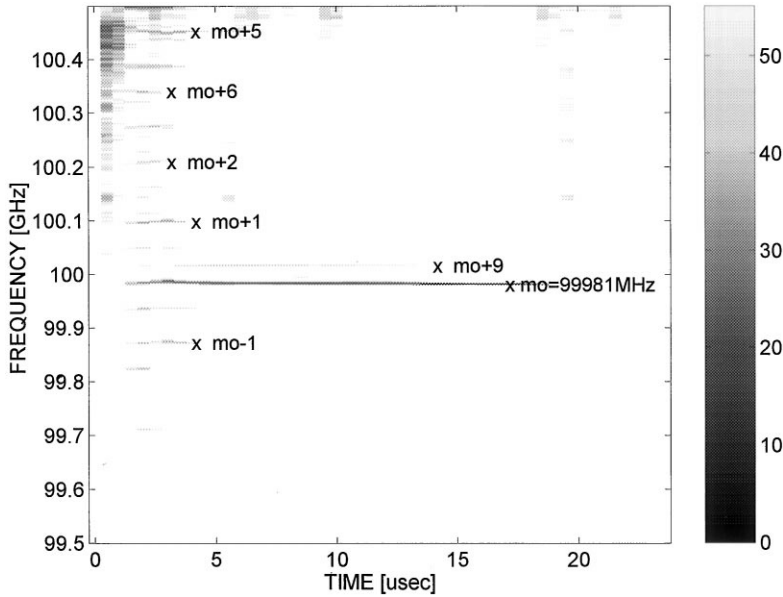


Fig. 4. Spectral analysis of the IF signal for single-mode operation at 99.981 GHz (where the gray scale is attenuation in dB and the maximum peak is normalized to 0 dB).

longitudinal mode frequencies;

$$f_{\text{IF}_m} = |f_m - f_{\text{LO}}| \quad (1)$$

where f_{LO} is the local oscillator frequency, f_m is the eigen-frequency of the FEL oscillator longitudinal mode m excited, and f_{IF_m} is the down converted IF signal. The gray scale is the attenuation in dB (the maximum peak was normalized to 0 dB). The spectral analysis shows that we obtain single-mode operation at an eigenfrequency of 99.981 GHz (marked m_0 in Fig. 4). Furthermore, we can see evidence of mode competition between longitudinal modes of the resonator at the beginning of the radiation build-up process. The free-spectral range (FSR) between the eigen-frequencies of the resonator is given by

$$\Delta f_{\text{FSR}} = v_g/2L_c \approx 112 \text{ MHz} \quad (2)$$

where v_g is the group velocity of the electromagnetic wave and L_c is the resonator length [8]. The spectrum shown in Fig. 4 is obtained by subtracting the local oscillator frequency from all of the IF components. Therefore, some of the components are image frequencies of the excited modes. Using experimental data obtained with differing local os-

cillator frequencies and with the calculated value of Δf_{FSR} we prove that the steady-state single frequency, which evolves at 99.981 GHz (marked as m_0 at Fig. 4), is the main mode eigenfrequency of the FEL oscillator. The components at 99.873 GHz is the $m_0 - 1$ mode, at 100.099 GHz is the $m_0 + 1$ mode and at 100.210 GHz is the $m_0 + 2$ mode. Other frequencies shown in Fig. 4 are the image frequencies resulting from mixing of the $m_0 + 5$, $m_0 + 6$ and $m_0 + 9$ eigenfrequencies of the FEL oscillator which are at 100.547 GHz, 100.658 GHz and 100.983 GHz, respectively.

During the e-beam pulse the voltage droops at the terminal by 22 kV (see Fig. 3), which causes the small signal gain curve to move towards lower frequencies. Using our 3D simulation code FEL 3D [9,10], the small signal gain of the FEL is calculated. Fig. 5 shows FEL 3D simulation code results of small signal gain of the EA-FEL for two values of the accelerating voltage; $V = 1.400$ MV and 22 kV lower ($V = 1.378$ MV), which correspond to the voltage droop in our experiment. The simulation results show that the frequency component m_0 at 99.981 GHz is still under the gain curve even after the voltage drops by 22 kV.

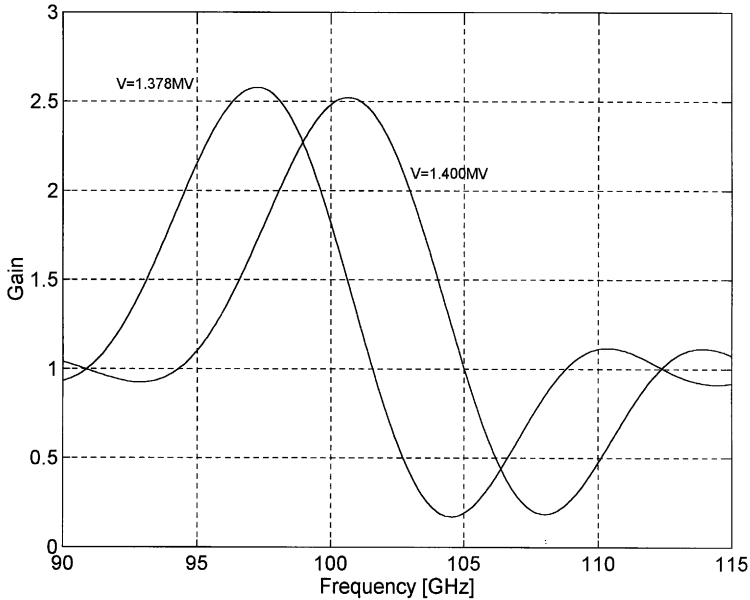


Fig. 5. FEL 3D simulation code results for small signal gain in two cases of accelerating voltages 1.4 and 1.378 MV which corresponds to the high voltage droop.

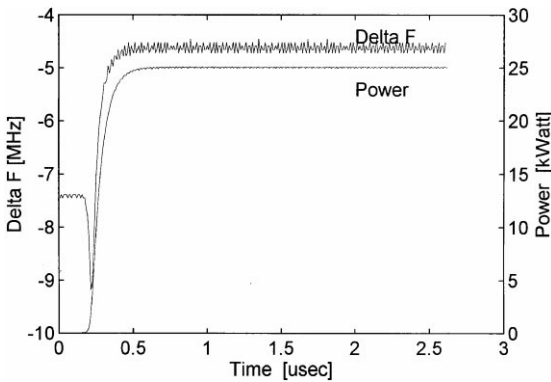


Fig. 6. Simulation results of radiation power buildup and frequency deviation.

The FEL 3D code was also used to simulate main mode radiation build-up from noise (spontaneous emission) level up to saturation. The initial spontaneous emission power (of the main mode) that was used in the simulation was $P_{sp}^{mode} = 1 \mu\text{W}$. This was calculated from analytical expression [11] using the parameters of Table 1.

Fig. 6 shows simulation results of power evolution and instantaneous frequency deviation (from the main mode frequency as a function of time). Inspection of Fig. 6 reveals that a transient frequency instability occurs as the oscillator reaches the non-linear regime and enters to saturation. This effect was also observed experimentally as shown in Fig. 7 and can be interpreted as a relaxation oscillation phenomenon [12].

Acknowledgements

This work was supported by the Israeli ministries of Energy and Science Foundation, and the Meyer Fund.

References

- [1] E. Jerby et al., Nucl. Instr. and Meth. A 259 (1987) 263.
- [2] A. Arensburg et al., Nucl. Instr. and Meth. A 375 ABS (1996) 1
- [3] A. Abramovich et al., Appl. Phys. Lett. 71 (1997) 26.

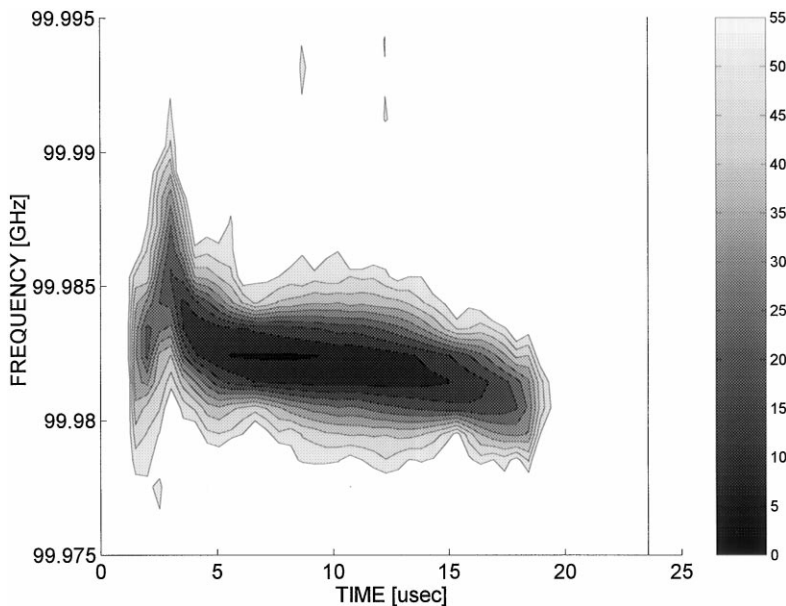


Fig. 7. Expansion of the time–frequency analysis of the recorded IF signal near the dominant mode.

- [4] I. Merhasine et al., Nucl. Instr. and Meth., 1998, submitted for publication.
- [5] K. Halback, Nucl. Instr. and Meth. A 169 (1980) 1.
- [6] A. Abramovich et al., Nucl. Instr. and Meth. A 407 (1998) 81.
- [7] B.C. Lee et al., Nucl. Instr. and Meth. A 375 (1996) 28.
- [8] I.M. Yakover, Y. Pinhasi, A. Gover, Nucl. Instr. and Meth. A 358 (1995) 323.
- [9] Y. Pinhasi et al., Int. J. Electron. 78 (1995) 581.
- [10] Y. Pinhasi et al., Phys. Rev. E 54 (1996) 6774.
- [11] A. Gover et al., in: K. Buttom (Ed.), Design Consideration for free electron lasers, Academic Press, New York, 1984.
- [12] A. Yariv, Quantum Electronics, third ed., Wiley, New York, 1989.